Atomic-Scale Friction on Diamond: A Comparison of Different Sliding Directions on (001) and (111) Surfaces Using MD and AFM

Guangtu Gao,[†] Rachel J. Cannara,[‡] Robert W. Carpick,[§,||] and Judith A. Harrison*[,†]

Chemistry Department, United States Naval Academy, Annapolis, Maryland 21402, Physics Department, University of Wisconsin−Madison, Madison, Wisconsin 53706, and Engineering Physics Department, University of Wisconsin−Madison, Madison, Wisconsin 53706

Received July 31, 2006. In Final Form: January 23, 2007

Atomic force microscopy (AFM) experiments and molecular dynamics (MD) simulations were conducted to examine single-asperity friction as a function of load, surface orientation, and sliding direction on individual crystalline grains of diamond in the wearless regime. Experimental and simulation conditions were designed to correspond as closely as state-of-the-art techniques allow. Both hydrogen-terminated diamond (111)(1 × 1)-H and the dimer row-reconstructed diamond (001)(2 × 1)-H surfaces were examined. The MD simulations used H-terminated diamond tips with both flat- and curved-end geometries, and the AFM experiments used two spherical, hydrogenated amorphous carbon tips. The AFM measurements showed higher adhesion and friction forces for (001) vs (111) surfaces. However, the increased friction forces can be entirely attributed to increased contact area induced by higher adhesion. Thus, no difference in the intrinsic resistance to friction (i.e., in the interfacial shear strength) is observed. Similarly, the MD results show no significant difference in friction between the two diamond surfaces, except for the specific case of sliding at high pressures along the dimer row direction on the (001) surface. The origin of this effect is discussed. The experimentally observed dependence of friction on load fits closely with the continuum Maugis−Dugdale model for contact area, consistent with the occurrence of single-asperity interfacial friction (friction proportional to contact area with a constant shear strength). In contrast, the simulations showed a nearly linear dependence of the friction on load. This difference may arise from the limits of applicability of continuum mechanics at small scales, because the contact areas in the MD simulations are significantly smaller than the AFM experiments. Regardless of scale, both the AFM and MD results show that nanoscale tribological behavior deviates dramatically from the established macroscopic behavior of diamond, which is highly dependent on orientation.

Introduction

The properties of diamond, such as excellent thermal conductivity, corrosion and wear resistance, and surface stability have made it the subject of tremendous scientific and technological interest.[1,2] The advent of chemical vapor deposition (CVD)[3] sparked interest in diamond as a thin film coating for flat panel displays, cutting tools, bearings, and micro- and nanoelectromechanical systems (MEMS/NEMS).[4] Its hardness and resistance to wear make it particularly attractive for tribological applications.[5] In these applications, the morphology of the diamond film is a critical factor in determining its performance.[6] Conventionally grown microcrystalline diamond (MCD) films are too rough to use without polishing[7] and often contain undesirable defects. It is now possible to grow nanocrystalline diamond (NCD) films[8,9] that have far smoother surfaces.[10] The decreased surface roughness of NCD reduces friction and wear[6] and makes it of significant interest for use in micro- and nanoelectromechanical systems (MEMS/NEMS).[11−13]

The macroscopic tribological properties of both single-crystal and polycrystalline diamond have been studied extensively.[14−16] Of particular interest here is the effect of orientation, which refers to both the crystallographic orientations of the contacting surfaces and the orientation of the sliding direction with respect to the crystallographic axes. It is well-established that friction and wear of diamond exhibits substantial orientation effects. This could have significant consequences if such effects occur at small scales, where interfaces may involve only a few discrete pairs of individual grains in contact. Thus, the tribological predictability and reliability of diamond-based MEMS/NEMS devices will be affected by the degree to which friction and wear vary with orientation. Furthermore, studies of the dependence of friction on orientation can provide insight into the fundamental mechanisms determining friction at all length scales.

Previous macroscopic studies of the influence of orientation on the tribological behavior of diamond predominantly focus on surface roughness effects, plastic deformation, and wear,[17−21]

* To whom correspondence should be addressed. E-mail: jah@usna.edu.

[†] United States Naval Academy.

[‡] Physics Department, University of Wisconsin−Madison.

[§] Engineering Physics Department, University of Wisconsin−Madison.

[||] Current address: University of Pennsylvania, Department of Mechanical Engineering and Applied Mechanics.

(1) Field, J. E. *The Properties of Diamond*; Academic Press: London, 1979.

(2) Field, J. E. *The Properties of Natural and Synthetic Diamond*; Academic Press: London, 1992.

(3) Celii, F. G.; Butler, J. E. *Annu. Rev. Phys. Chem.* **1991**, *42*, 643.

(4) Tang, W. C.; Lee, A. P. *Mater. Res. Soc. Bull.* **2001**, *26*, 318.

(5) Erdemir, A.; Donnet, C. Tribology of Diamond, Diamond-Like Carbon, and Related Films. In *Modern Tribology Handbook*; Bhushan, B., Ed.; CRC Press LLC.: Boca Raton, FL, 2001; Vol. 2, pp 871.

(6) Hayward, I. P.; Singer, I. L.; Seitzman, L. E. *Wear* **1992**, *157*, 215.

(7) Gardos, M. N. *Surf. Coat. Technol.* **1999**, *113*, 183.

(8) Gruen, D. M. *Annu. Rev. Mater. Sci.* **1999**, *29*, 211.

(9) Philip, J.; Hess, P.; Feygelson, T.; Butler, J. E.; Chattopadhyay, S.; Chen, K. H.; Chen, L. C. *J. Appl. Phys.* **2003**, *93*, 2164.

(10) Sumant, A. V.; Grierson, D. S.; Gerbi, J. E.; Birrell, J.; Lanke, U. D.; Auciello, O.; Carlisle, J. A.; Carpick, R. W. *Adv. Mater.* **2005**, *17*, 1039.

(11) Erdemir, A.; Bindal, C.; Fenske, G. R.; Zuiker, C.; Csencsits, R.; Krauss, A. R.; Gruen, D. M. *Diamond Relat. Mater.* **1996**, *6*, 31.

(12) Erdemir, A.; Bindal, C.; Fenske, G. R.; Zuiker, C.; Krauss, A. R.; Gruen, D. M. *Diamond Relat. Mater.* **1999**, *5*, 923.

(13) Popov, C.; Kulisch, W.; Jelinek, M.; Bock, A.; Strnad, J. *Thin Solid Films* **2006**, *494*, 92.

(14) Field, J. E.; Pickles, C. S. J. *Diamond Relat. Mater.* **1996**, *5*, 625.

(15) Feng, Z.; Tzeng, Y.; Field, J. E. *J. Phys. D. Appl. Phys.* **1992**, *25*, 1418.

(16) Grillo, S. E.; Field, J. E. *Wear* **2003**, *254*, 945.

(17) Enomoto, Y.; Tabor, D. *Proc. R. Soc. London A* **1981**, *373*, 405.

(18) Grillo, S. E.; Field, J. E. *J. Phys. D. Appl. Phys.* **2000**, *33*, 595.

10.1021/la062254p CCC: $37.00
Published on Web 04/04/2007

and they are concerned primarily with the polishing of diamond. They typically explore only a few specific loads in the range of microNewtons, and the actual contact areas and pressures are unknown. Tolkowsky was the first to investigate the anisotropy of the friction coefficient and wear on single-crystal diamond,[21] and subsequent observations have confirmed his basic results.[17−20] For {001} surfaces, friction coefficients are highest along the ⟨001⟩ directions, which exhibit chemical wear as opposed to the chipping wear that occurs along the ⟨110⟩ directions. The ⟨001⟩ directions are softer and more easily worn than other sliding directions, and the {001} surfaces are more easily polished along the ⟨001⟩ directions. Likewise, for the {110} surfaces, the ⟨001⟩ directions are the softest. The {111} surfaces have the lowest friction coefficients, are the most difficult to polish regardless of direction, and exhibit a slight threefold anisotropy. This summarizes the extent to which experts agree on the macroscopic wear properties of single-crystal diamond. Disagreements stem from variations in experimental conditions, leading to different results for wear-rates and coefficients of friction as a function of sliding speed and (apparent) contact pressure.

Although the macroscopic tribological behavior of MCD and NCD films has been reported,[6,7] there have been only limited efforts to study orientation effects. In their pin-on-disc experiments, Schmitt et al. compared (001)- and (111)-oriented MCD coated pins sliding on stainless steel discs at two different loads (0.2 and 1.4 N) and in several environments (oxygen, water vapor, and vacuum).[22] The tribological properties of both coatings were similar, except at low load in humid conditions. In that case, the (001) friction coefficient was approximately 5 times lower than for (111). The interpretation is ambiguous because the samples differed in grain size and roughness, and the testing conditions were not held constant. Other investigations have begun to address the issue of surface orientation at the microscale.[23] However, orientation is not controlled independently of other parameters, such as roughness, grain size, degree of sp^3 coordination, etc. With so many different mechanisms at play, there is a significant need to gain greater control in experiments and simulations. Nanoscale AFM measurements and MD simulations provide an opportunity to vary individual parameters (e.g., load, contact pressure on smooth surfaces, sliding direction, sliding speed, and environment) and add insight into the fundamental friction mechanisms for diamond. In fact, in their review of the macroscale tribological properties of diamond, Field and Pickles encouraged scientists to use AFM and MD for these reasons.[15]

AFM has been used in a few cases to examine diamond tribology.[24−29] In the only AFM-based study of surface orientation to date, wearless friction was measured in UHV between a CVD-grown diamond crystallite on the end of a tungsten-wire cantilever and single-crystal diamond (111) and (001) surfaces.[29] The tip was oriented so that a sharp corner of the crystallite made contact with the samples. The samples were polished and annealed using a method to H-terminate the surface, and atomic-scale stick-slip friction was observed. The sliding directions were not aligned with any particular crystallographic direction, but friction forces between the tip and both surfaces were similar and independent of load up to 10 μN.

The AFM was also used to measure friction and contact area as a function of load between a tungsten carbide tip and hydrogen-terminated diamond (111) in UHV.[24] The measured local contact conductance between the tip and the sample demonstrated that friction was proportional to contact area as described by the Derjaguin−Muller−Toporov (DMT) model.

Finally, Schwarz et al. studied single-asperity friction in air and in argon on individual grains of (001)-oriented CVD MCD using a hydrocarbon-coated tip.[26] They also observed that friction was proportional to the area of contact predicted by a continuum mechanics model. Because the elastic constants of their tip were unknown, an effective shear strength (or "effective friction coefficient"), which represents a combination of the interfacial shear strength and the elastic properties of the tip and sample, was extracted. This allowed a relative comparison of different surfaces by using the same tip. They found that diamond exhibits moderate effective shear strengths in the wearless regime relative to other carbon-based compounds. Interestingly, they found that friction is greater in air than in dry argon, though there was no attempt to hydrogen-terminate the MCD surface after CVD growth.

MD has also been used in the past to study friction of diamond interfaces, but to date, all previous work has used infinitely flat diamond counterfaces and the first-generation reactive empirical bond-order (REBO) potential.[30,31,33] For self-mated, crystallographically aligned diamond (111) surfaces, friction increases with load when sliding in either the $[11\bar{2}]$ direction or the $[1\bar{1}0]$ direction. However, due to different relative starting positions of the opposing crystal surfaces and, perhaps, because of the planar geometry of the surfaces, the $[\bar{1}10]$ direction gave slightly lower friction force than the $[11\bar{2}]$ direction ($\mu = 0-0.4$). Subsequent ab initio studies of atomic-scale friction between $C_{13}H_{22}$ clusters, which are analogs to hydrogen-terminated diamond (111) surfaces, reported a friction coefficient (0.22)[32] when sliding in the direction which was comparable to the values obtained in the earlier simulations.

Also, the average friction force between self-mated infinitely flat diamond (001)(2×1) surfaces in the $[\bar{1}10]$ and [110] the directions was found to be approximately equal to the average friction force on the (111) surface when sliding in the $[11\bar{2}]$ direction.[33] In that work, friction coefficients were averaged over starting configurations that differed in the initial relative positions of the crystals (i.e., whereas the crystallographic axes were aligned directionally, different lateral positional offsets were used as the starting configurations). The friction force varied periodically with the atomic lattice, and the maxima corresponded to points of strong interaction between hydrogen atoms on opposing surfaces.[33] The vibrational excitation (heating) of the surface bonds generated by this interaction is the essence of wearless atomic-scale friction on diamond.

Although these early MD studies were the first of their kind on diamond, there are several ways in which the simulation conditions were not well-matched to nanoscale experiments. Most importantly, both contacting surfaces were infinitely flat. Thus,

(19) Hird, J. R.; Field, J. E. *Proc. R. Soc. London A* **2004**, *460*, 3547.
(20) Seal, M. *Proc. R. Soc. London A* **1958**, *248*, 379.
(21) Tolkowsky, M. *Research on the abrading, grinding or polishing of diamond*; University of London: London, 1920.
(22) Schmitt, M.; Paulmier, D.; Huu, T. L. *Thin Solid Films* **1999**, *343−344*, 226.
(23) Forbes, I. S.; Wilson, J. I. B. *Thin Solid Films* **2002**, *420−421*, 508.
(24) Enachescu, M.; van den Oetelaar, R. J. A.; Carpick, R. W.; Ogletree, D. F.; Flipse, C. F. J.; Salmeron, M. *Phys. Rev. Lett.* **1998**, *81*, 1877.
(25) Enachescu, M.; van den Oetelaar, R. J. A.; Carpick, R. W.; Ogletree, D. F.; Flipse, C. F. J.; Salmeron, M. *Tribol. Lett.* **1999**, *7*, 73.
(26) Schwarz, U. D.; Zworner, O.; Koster, P.; Wiesendanger, R. *Phys. Rev. B* **1997**, *56*, 6987.
(27) van den Oetelaar, R. J. A.; Flipse, C. F. J. *Surf. Sci.* **1997**, *384*, L828.
(28) Zworner, O.; Holscher, H.; Schwarz, U. D.; Wiesendanger, R. *Appl. Phys. A* **1998**, *66*, S263.
(29) Germann, G. J.; Cohen, S. R.; Neubauer, G.; McClelland, G. M. *J. Appl. Phys.* **1993**, *73*, 163.
(30) Harrison, J. A.; White, C. T.; Colton, R. J.; Brenner, D. W. *Phys. Rev. B* **1992**, *46*, 9700.
(31) Perry, M. D.; Harrison, J. A. *J. Phys. Chem. B* **1997**, *101*, 1364.
(32) Neitola, R.; Pakkanen, T. A. *J. Phys. Chem. B* **2001**, *105*, 1338.
(33) Perry, M. D.; Harrison, J. A. *J. Phys. Chem.* **1995**, *99*, 9960.

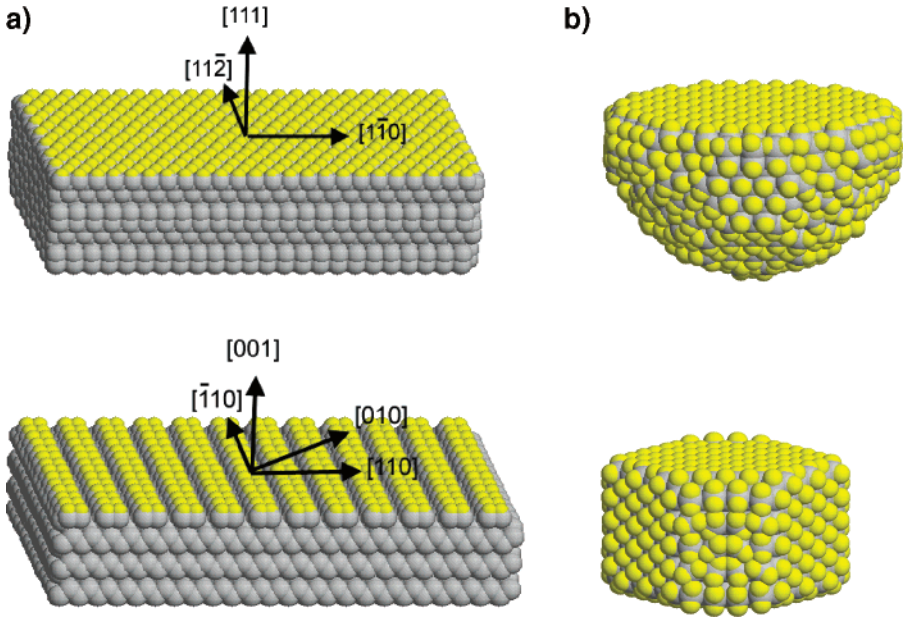

Figure 1. Surfaces and tips used. (a) The (111) and (001) diamond surfaces used in the simulations and the experiments are shown in the upper and lower panels, respectively. The crystallographic sliding directions are shown by arrows. (b) The curved and nanowire diamond tips shown in the upper and lower panels, respectively. The tips themselves are viewed from the side, and the surfaces contacting the diamond substrates are at the bottom of the tips.

the application of load causes the uniform compression of both materials over a constant contact area, rather than nonuniform compression of the materials and a varying contact area with load, which occurs with a curved surface such as an asperity or an AFM tip. Despite this, several insights into the friction of diamond against diamond were obtained. For example, friction in the presence of third-body molecules,[31,34] as a function of surface roughness,[35,36] sliding speed,[30,33] and temperature[30] were all examined. Specific energy dissipation mechanisms[34,37] and tribochemical reactions[38] that occur during sliding were identified. Subsequently, a number of the phenomena identified in these early works have been examined with quantum calculations using various levels of approximation.[32,39,40]

In this work, we take a significant step toward more closely matching experimental conditions by using finite, curved geometries. Furthermore, the simulations make use of the second-generation REBO potential[41] which, in contrast to the first-generation REBO potential, reproduces the zero-Kelvin elastic constants of diamond and graphite accurately. Because the extraction of shear strengths from AFM data using continuum theory requires knowledge of the mechanical properties of the tip and the sample, the accurate modeling of the elastic properties is central to the correspondence between the simulations and the experiments. Significant differences in sliding speed and tip size still exist between simulation and experiment. This can only be overcome by increasing algorithmic efficiency and computer run times by several orders of magnitude. This is a universal challenge faced by all efforts to compare atomistic simulations with experiments. Rather than refraining from considering any results, we discuss the limitations imposed by these differences and explore the physical insights that are, nonetheless, provided by correspondences and disagreements in the MD and AFM results.

Methods

Joint AFM experiments and MD simulations of nanoscale friction as a function of load for (111)- and (001)-oriented crystalline grains were performed. Because these are the two most stable surfaces of diamond, they are the most likely to be expressed in polycrystalline diamond films. The experiments used a hydrogen-terminated MCD sample grown specifically for these experiments. The micrometer size of the grains allowed friction on individual (111) and (001) grains to be examined independently by AFM. With that in mind, hydrogen-terminated diamond (111) and (001) samples were both examined using MD simulations.

Two amorphous hydrocarbon-coated AFM tips with nearly atomically smooth, round shapes were used for these experiments. The MD simulations used two hydrogen-terminated crystalline diamond tips with different geometries. One is a round tip carved from a (111)-oriented crystal, and the other has a flat (110) orientation. The details are specified in the next section. Although it would be preferable to create amorphous hydrocarbon tips for the MD simulations to match the experiments, the unknown composition and bonding characteristics of the AFM tips renders such an approach equally subject to uncertainty for comparison purposes. As well, designing crystalline diamond AFM tips with prescribed orientations is impractical. We discuss the limitations imposed by the differences in MD and AFM tips further below.

Specific high-symmetry crystallographic sliding directions were prescribed on both surfaces such that a total of five different surface-orientation/sliding-direction combinations were studied. Because the MCD grains are randomly oriented, AFM experiments on any particular surface-orientation/sliding-direction combination require locating facets with the appropriate orientations (both the surface normal and the sliding direction) within a limited range of acceptable tilt angles with respect to the AFM's $x-y$ scanning plane. Furthermore, making reliable comparisons of different orientations/directions requires being able to sequentially alternate between the desired grains using the same tip. Thus, at least two such positions

(34) Perry, M. D.; Harrison, J. A. *Tribol. Lett.* **1995**, *1*, 109.
(35) Harrison, J. A.; White, C. T.; Colton, R. J.; Brenner, D. W. *J. Phys. Chem.* **1993**, *97*, 6573.
(36) Harrison, J. A.; Colton, R. J.; White, C. T.; Brenner, D. W. *Wear* **1993**, *168*, 127.
(37) Harrison, J. A.; White, C. T.; Colton, R. J.; Brenner, D. W. *Thin Solid Films* **1995**, *260*, 205.
(38) Harrison, J. A.; Brenner, D. W. *J. Am. Chem. Soc.* **1994**, *116*, 10399.
(39) Dag, S.; Ciraci, S. *Phys. Rev. B* **2004**, *70*, 241401(R).
(40) Koskilinna, J. O.; Linnolahti, M.; Pakkanen, T. A. *Tribol. Lett.* **2005**, *20*, 157.
(41) Brenner, D. W.; Shenderova, O. A.; Harrison, J. A.; Stuart, S. J.; Ni, B.; Sinnott, S. B. *J. Phys. C* **2002**, *14*, 783.

must be found within a few μm of each other so that they can be accessed using the AFM piezo scanner. Due to this difficult challenge, a subset of the combinations was examined with each AFM tip, although all five combinations were measured in total.

On the (111) surface, the close-packed [1$\bar{1}$0] direction and the direction perpendicular to it, [11$\bar{2}$], were studied (Figure 1a). On the (001) surface, the [010], the close-packed [$\bar{1}$10], and the close-packed [110] directions were studied. The last two directions would be identical on an unreconstructed (1 × 1) surface. However, the H-terminated (001) surface exhibits a (2 × 1) reconstruction that forms domains of dimer rows that align parallel to either the [$\bar{1}$10] or [110] direction.[42,43] This structure has been shown to be energetically favorable over the (1 × 1) dihydride structure.[44] The (2 × 1) structure is illustrated in Figure 1, where we have chosen to place the dimer bonds along the [110] direction. MD simulations can examine physical properties that are difficult to measure experimentally. For instance, the size of the domains on the (001) surface and the size of typical AFM tips make it difficult to examine friction parallel and perpendicular to the dimer rows independently. The simulations suffer from no such constraints, and the dependence of friction on dimer orientation was investigated.

The AFM measurements were conducted in a dry nitrogen environment (<5% relative humidity, corresponding to the limit of the measuring device), using a Digital Instruments MultiMode AFM with a Nanoscope IV controller. This AFM uses optical beam deflection to record the normal and lateral signals from a four-quadrant photosensitive detector (PSD).[45] These signals are proportional to forces between the AFM cantilever probe tip and sample surface. Quantitative nanotribology measurements were obtained with two different probe tips with curved apexes with radii of 45 ± 3 and 150 ± 10 nm. The tips were formed by coating the tips of tungsten carbide-coated silicon cantilever probes (MikroMasch, Wilsonville, OR) with a smooth hydrogenated amorphous carbon film using electron beam induced decomposition (EBID) in a transmission electron microscope (TEM).[46,47] This process forms a dense hydrocarbon coating on the tip, but the exact composition and hybridizations of the carbon atoms are not known. Both tips were imaged at high resolution by TEM before and after the AFM experiments to measure tip shape and radius and to determine the extent to which the tip may have changed during the experiment. Wear was either unobservable (with the 150 nm tip) or extremely small (with the 45 nm tip), and a rounded apex was maintained in both cases (Figure 2). No roughness or waviness of the surface of the tip was observable. Recent work has established a physical basis for atomic-level smoothness of hydrocarbon films grown by decomposition reactions,[46] and such a mechanism is likely at play here. Sliding speeds were 1.22 μm/s (at a rate/scan length of 30.5 Hz/20 nm and 61 Hz/10 nm for the 150 and 45 nm tips, respectively).

MCD films with an abundance of (001)- and (111)-oriented grains were grown and hydrogen-terminated using standard procedures in a custom-built hot filament chemical vapor deposition (HF−CVD) system described elsewhere.[48] A scanning electron microscope (SEM) image of the MCD film used in this work is shown in Figure 3. The MCD films were comprehensively characterized using a sophisticated array of surface science techniques. The results will be reported in detail elsewhere. Briefly, Raman spectroscopy, near-edge X-ray absorption fine structure spectroscopy, sum frequency generation, and elastic recoil detection were used to unambiguously verify the high quality of the diamond films and the hydrogen termination procedure. SEM images and AFM topography measurements show

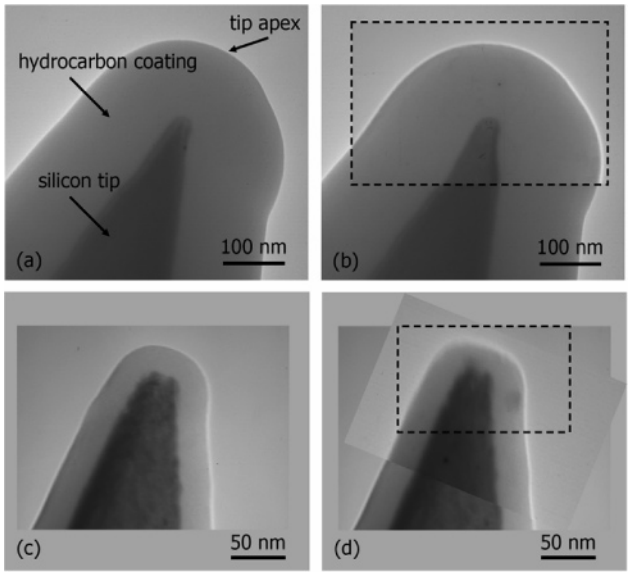

Figure 2. TEM images of the hydrocarbon-coated AFM tips before and after friction vs load measurements. The 150 nm tip is shown (a) before and (b) after the experiment. The dotted-line region in panel b is the "after" image overlaid on panel a. There is a slight difference in Si substrate shape, but this is an artifact of the focus and sample position in the TEM. Panels c and d are before and after images of the 45 nm tip, respectively. The dotted-line region in panel d is the "after" image overlaid on panel c. No significant tip changes occurred that were apparent within the range accessible by TEM.

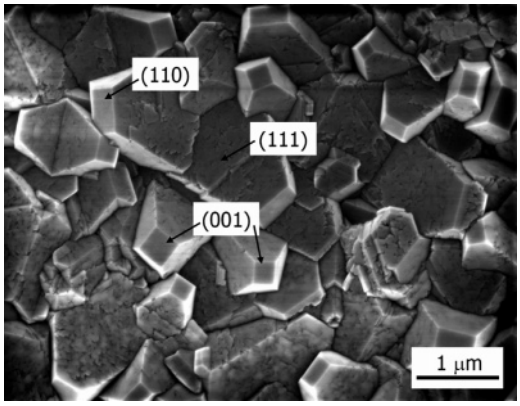

Figure 3. SEM image of the MCD film grown by HF−CVD, showing (111)-, (001)-, and (110)-oriented grains. Examples of different orientations are indicated.

that these films have 100-nm^2- to 1-μm^2-sized grains of random orientation with respect to the substrate, but with an equal distribution of (001) and (111) surface orientations. The H-terminated surfaces of the (111) and (001) crystallite grains contain atomically smooth 10−50-nm-diameter islands that form due to etching by atomic hydrogen.

A sequence of multiple, alternating measurements between selected pairs of crystallites with different orientations enabled us to reliably compare interfacial properties independent of changes in the tip or environment (e.g., humidity or temperature) that could occur over long time periods. For each surface and sliding direction combination, a series of at least 25 friction vs. load scans were taken, repeatedly alternating between combinations every 5 scans. Fits to the individual friction vs. load data produced values for the work of adhesion and effective shear strength, as discussed in the Results section. Normal and lateral forces were calibrated using the Sader and wedge force calibration methods, respectively.[49−51] Error bars for friction data

(42) Stallcup, R. E., II; Villareal, L. M.; Lim, S. C.; Akwani, I.; Aviles, A. F.; Perez, J. M. *J. Vac. Sci. Technol. B* **1996**, *14*, 929.
(43) Wang, Y. M.; Wong, K. W.; Lee, S. T.; Nishitani-Gamo, M.; Sakaguchi, I.; Loh, K. P.; Ando, T. *Phys. Rev. B* **1999**, *59*, 10347.
(44) Davidson, B. N.; Pickett, W. E. *Phys. Rev. B* **1994**, *49*, 11253.
(45) Meyer, G.; Amer, N. M. *Appl. Phys. Lett.* **1990**, *57*, 2089.
(46) Ding, W.; Dikin, D. A.; Chen, X.; Piner, R. D.; Ruoff, R. S.; Zussman, E. *J. Appl. Phys.* **2005**, *98*, 014905.
(47) Schwarz, U. D.; Zworner, O.; Koster, P.; Wiesendanger, R. *J. Vac. Sci. Technol. B* **1997**, *15*, 1527.
(48) Yap, H.-W.; Ramaker, B.; Sumant, A. V.; Carpick, R. W. *Diamond Relat. Mater.* **2006**, *15*, 1622.
(49) Cannara, R. J.; Eglin, M.; Carpick, R. W. *Rev. Sci. Instrum.* **2006**, *77*, 53701.

Table 1. Details of the Surfaces and Sliding Directions Used

			MD parameters				
surface	sliding direction	AFM tips used	# of carbon atoms	# of hydrogen atoms	*X* size (Å)	*Y* size (Å)	*Z* size (Å)
(111) (1 × 1)-H	[1$\bar{1}$0]	150 nm, 45 nm	4992	384	60.5	34.9	13.35
(111) (1 × 1)-H	[11$\bar{2}$]	45 nm	5096	392	35.3	61.1	13.35
(001) (2 × 1)-H	[$\bar{1}$10]	150 nm,[a] 45 nm[a,b]	5096	392	35.3	70.6	11.75
(001) (2 × 1)-H	[110]	150 nm,[a] 45 nm[a,b]	4368	336	60.5	35.3	11.75
(001) (2 × 1)-H	[010]	150 nm	3328	256	40.3	40.3	11.75

[a] The [$\bar{1}$10] and [110] directions could not be distinguished in the AFM measurements. [b] The experiments on the (001) surface with the 45 nm tip produced only limited friction data that could be analyzed.

were calculated by combining the standard error on the mean (standard deviation divided by the square root of the number of averaged data points) with a 4.2% uncertainty in the lateral force calibration. The error in normal forces in these experiments was smaller than the data points plotted.

To examine the effects of tip geometry, two model diamond tips were used in the simulations (Figure 1b). The first, referred to as a diamond nanowire tip, was composed of 10 layers of (110) diamond with {110} and {001} sidewalls. It contained 840 sp^3-bonded carbon atoms, and its outer surfaces were terminated with 360 hydrogen atoms in (1 × 1) configurations, eliminating unsaturated carbon bonds. It had an irregular hexagonal shape with a radius of approximately 11.4 Å and a thickness of 14.5 Å. In an effort to replicate the shape of the AFM tip, the second tip was constructed from a diamond (111) crystal by removing atoms to make the tip roughly hemispherical (radius = 15 Å). Hydrogen atoms were added to saturate all bonds on the tip surface. This tip contains 1352 sp^3-bonded carbon atoms and 520 hydrogen atoms. Knowledge of the shape of the AFM tip is paramount to extracting quantitative data from AFM experiments. Although computational power limits our ability to simulate a tip of the same size as those in the experiment, this approach at least allows us to consider the effect that tip geometry (finite round or finite flat vs infinite flat) has on the friction-load relation.

For uniformity, the [1$\bar{1}$0] direction of the nanowire tip was always aligned with the sliding direction along the sample. Thus, the nanowire tip is commensurate with all sliding directions except for the (111) surface when sliding in the [11$\bar{2}$] direction and the (001) surface when sliding in the [010] direction. In contrast, the curved tip is stepped and incommensurate with both diamond surfaces in all sliding directions. Both of these tips were used to examine friction of diamond (111)(1 × 1)-H and (001)(2 × 1)-H as a function of load.

The (111)- and the (001)-oriented samples both have 13 layers of carbon (Figure 1). For each sliding simulation, the sample was made slightly wider in the sliding direction. Table 1 summarizes the total number of atoms in each sample, the dimensions, and the sliding directions. The samples were partitioned into 3 regions. The atoms in the farthest layer from the interface were held fixed. The atoms in the middle region had a thermostat applied to maintain the temperature of the simulation at 300 K.[52] The atoms closest to the sliding interface had no constraints and were integrated according to Newton's equations of motion. The time step for all the simulations was 0.25 fs. All tip atoms were held rigid. That is, the equations of motion are not integrated for these atoms. This was done so that frictional differences between tips could be assigned to geometric differences and not differences in the dynamics of the tip atoms. The whole tip was treated as a rigid body, and an external force was applied on the tip toward the diamond sample to simulate a system under a constant external-load condition.

Periodic boundary conditions were applied in the plane containing the surface. The tip dimensions were chosen so that it did not interact with its periodic image. Dimensions of the sample were selected to be as large as possible while remaining computationally feasible. Because many simulations are required, this number must be considered when selecting the simulation size. Indeed, the MD tips are an order of magnitude smaller than the AFM tips, and the MD sliding speeds are 6 orders of magnitude greater than the AFM speeds. These are universal issues for state-of-the-art MD and AFM measurements currently. The sliding speeds in both cases are below the speed of sound of diamond (4 orders of magnitude for the MD simulations, for example), and so, we do at least expect that we are not encountering dynamical effects due to the resonant inducement of sound waves.

In the indentation simulations, tips are placed above the diamond surfaces at a distance where the potential energy equals zero and then moved at a constant speed of 1.0 m/s toward the diamond surfaces. Sliding simulations are performed by moving the tip parallel to the diamond substrate at a constant speed, with an external constant force on the tip. Tip speeds of 0.84 and 1.0 m/s were both used. As the tip slides, the friction force oscillates in periodic cycles about an average value. Tip speeds were chosen so that the friction force experiences an integer number of complete oscillation cycles within each unit cell. Governed by the dynamic equations from Newton's Second Law, the tip will oscillate around an average height relative to the film, resulting in an average load on the film equal to the constant force on the tip.[53]

These simulations utilize the second-generation REBO potential, which was parametrized to model solid and gas-phase hydrocarbon systems and is capable of modeling chemical reactions.[41] Thus, it is possible to observe the formation and breaking of bonds that can accompany sliding in simulations that utilize this potential. The second-generation REBO, and its predecessor, have been used to model the mechanical properties of filled and unfilled nanotubes,[54] the tribochemistry of diamond surfaces and chemically bound hydrocarbon chains,[38] the friction and wear of amorphous carbon films,[55] and the stress at grain boundaries.[56] Recently, the second-generation REBO potential was shown to accurately reproduce the 0 K elastic constants of diamond and graphite[57] and qualitatively reproduces the trends in elastic constants of diamond as a function of temperature.[58]

No long-range intermolecular forces (i.e., van der Waals or dipole forces) are included in this potential. Therefore, in the absence of any exposed unsaturated bonds at the interface, no adhesive interactions are present in the simulations. Although there is no adhesion in these MD simulations, they are still a valid approximation for DMT behavior because an adhesion term simply shifts the load by the pull-off force. The adaptive intermolecular REBO (AIREBO) potential is an extension of the second-generation REBO potential that includes intermolecular forces.[59] However, simulations conducted with AIREBO are approximately 7 times slower than those conducted

(50) Ogletree, D. F.; Carpick, R. W.; Salmeron, M. *Rev. Sci. Instrum.* **1996**, *67*, 3298.
(51) Sader, J. E. *Rev. Sci. Instrum.* **1999**, *70*, 3967.
(52) Berendsen, H. J. C.; Postma, J. P. M.; van Gunsteren, W. F.; DiNola, A.; and Haak, J. R. *J. Chem. Phys.* **1984**, *81*, 3684.
(53) Lupkowski, M.; van Swol, F. *J. Chem. Phys.* **1990**, *93*, 737.
(54) Ni, B.; Lee, K. H.; Sinnott, S. B. *J. Phys. Condens. Matter* **2004**, *16*, 7261.
(55) Gao, G. T.; Mikulski, P. T.; Harrison, J. A. *J. Am. Chem. Soc.* **2002**, *124*, 7202.
(56) Shenderova, O. A.; Brenner, D. W. *Solid State Phenom.* **2002**, *87*, 205.
(57) Van Workum, K.; Gao, G. T.; Schall, J. D.; Harrison, J. A. *J. Chem. Phys.* **2006**, *125*, 144506.
(58) Gao, G. T.; van Workum, K.; Schall, J. D.; Mikulski, P. T.; Harrison, J. A. *J. Phys. Condens. Matter*. **2006**, *18*, S1737.
(59) Stuart, S. J.; Tutein, A. B.; Harrison, J. A. *J. Chem. Phys.* **2000**, *112*, 6472.

Table 2. AFM Results for Normal Pull-Off Force during Scanning, Work of Adhesion, Friction Force at Zero Load, Effective Shear Strength ($\tilde{C}$), and Estimates for Shear Strengths, Ideal Shear Strengths, and Mean Contact Pressures for a Reasonable Range of Estimated Tip Moduli for the Different Surface Orientations and Sliding Directions[a]

surface	sliding direction	tip radius/ nm	scanning pull-off force/nN	work of adhesion/ J m^{-2}	friction force at zero load/ nN	effective shear strength $\tilde{C}$/nN$^{1/3}$nm$^{-2/3}$	tip Young's modulus (estimates) E_2/GPa	shear strength (estimates) τ_0/MPa	ideal shear strength (estimates) G*/30/ GPa	mean contact pressure @ 100 nN (estimates)/ GPa
(111) (1×1)-H	[11$\bar{2}$]	**45**	**29.7 ± 3.9**	**0.131 ± 0.025**	**5.6 ± 0.7**	**0.024 ± 0.002**	**100**	**201 ± 20**	**2**	**1.76 ± 0.14**
							500	**485 ± 49**	**9**	**4.26 ± 0.33**
	[1$\bar{1}$0]	**45**	**25.3 ± 1.9**	**0.103 ± 0.012**	**5.0 ± 0.6**	**0.026 ± 0.004**	**100**	**213 ± 34**	**2**	**1.86 ± 0.12**
							500	**514 ± 81**	**9**	**4.49 ± 0.28**
	[1$\bar{1}$0]	*150*	*27.6 ± 2.3*	*0.036 ± 0.005*	*7.4 ± 0.8*	*0.015 ± 0.002*	*100*	*121 ± 14*	*2*	*0.80 ± 0.05*
							500	*292 ± 35*	*9*	*1.92 ± 0.12*
(001) (2×1)-H	[$\bar{1}$10] or [110]	**45**	**53.6 ± 3.2**	**0.258 ± 0.030**	**6.5 ± 0.6**	**0.017 ± 0.002**	**100**	**140 ± 18**	**2**	**1.40 ± 0.10**
							500	**331 ± 44**	**10**	**3.32 ± 0.23**
		150	*45.0 ± 2.4*	*0.064 ± 0.006*	*11.4 ± 1.1*	*0.014 ± 0.002*	*100*	*119 ± 14*	*2*	*0.67 ± 0.04*
							500	*281 ± 33*	*10*	*1.57 ± 0.10*
	[010]	*150*	*48.1 ± 2.1*	*0.066 ± 0.006*	*11.0 ± 0.8*	*0.014 ± 0.002*	*100*	*116 ± 13*	*2*	*0.63 ± 0.04*
							500	*275 ± 31*	*10*	*1.57 ± 0.09*

[a] Experimental values for the elastic constants of diamond (001) and (111) are used to estimate contact areas, pressures, and shear strengths. The Young's moduli, shear moduli, and Poisson's ratios of diamond are, respectively: $E(001) = 1054$ GPa, $E(111) = 1208$ GPa, $G(001) = 577$ GPa, $G(111) = 506$ GPa, $\nu(001) = 0.105$, and $\nu(111) = 0.047$.[61,62] The hydrocarbon tips are assumed to be homogeneous, isotropic, linear, elastic materials. Therefore, $G_{tip} = E_{tip}/2(1 + \nu_{tip})$, where we have assumed a Poisson's ratio $\nu_{tip} = 0.3$. The effective shear modulus $G^* = 2G_{surf}G_{tip}/(G_{surf} + G_{tip})$. Italic and bold entries are data for the 150 and 45 nm tips, respectively. The numbers for $\tilde{C}$, work of adhesion (γ), and the friction force at zero load for the 45 nm tip on the (001) surface are based on fits to low-load data only, because the surface was highly tilted. However, all pull-off force data are directly measured.

with the REBO potential. Previous work has shown that for wearless friction between two infinitely flat surfaces, the AIREBO and the REBO potentials yield similar results for friction when plotted as a function of surface separation.[55] However, due to the long-range interactions, the load on the counterface is not the same at a given separation and so actual values of the normal forces obtained from each potential differ. Nevertheless, qualitative trends remain the same, and so the REBO potential was chosen for the simulations presented here. As an additional check, a small number of simulations were performed for the curved tip using both the AIREBO and the REBO potentials. The qualitative trends obtained were the same with both potentials.

The reported friction forces were obtained by averaging data from two sliding simulations with independent starting configurations. These two configurations were obtained by translating the tip a fraction of a unit-cell distance in the direction perpendicular to the sliding direction. For each individual simulation, the instantaneous friction force (force in the sliding direction) on the tip was recorded every 1 fs. The sliding distance was divided into unit-cell segments (based on the diamond surface), and the instantaneous forces were averaged over these unit-cell segments. The values for each unit-cell segment were then averaged to obtain an average friction force for a given simulation. In an AFM experiment, the tip is rastered over the sample (i.e., each scan line is obtained by incrementing the in-plane displacement perpendicular to the sliding direction) and so measurements are obtained over a range of relative positions between the tip and sample. Thus, averaging over different starting configurations approximates the line-averaged response from an AFM experiment.

The AFM and MD studies were carried out in the wearless friction regime so that the physical properties of the atomically smooth contacting surfaces, not of the wear debris or a transfer film, were examined. For the experiments, the magnitude of the maximum applied load was chosen to be approximately twice the pull-off force and was typically limited to ~100 nN. Because the elastic constants of the tip material are not known, we cannot determine the continuum mechanics prediction for the contact area or the contact stresses. However, based on a reasonable range of values for the elastic constants the mean contact pressures estimated by continuum mechanics at the typical upper load of 100 nN can be estimated. Using the average values for the Young's modulus and Poisson's ratio of diamond[60−62] given in Table 2 and assuming the tip moduli fall between 100 and 500 GPa with a Poisson's ratio of ~0.3, the combined elastic contact modulus K ranges from 133 to 504 GPa. If the continuum fits discussed below are used to model the load dependence of the contact area, then the maximum mean contact pressures applied in the experiments range between 0.6−1.9 and 1.4−4.5 GPa for the 150 and 45 nm tips, respectively (Table 2).

A rough comparison of the maximum AFM and MD mean contact pressures was made by choosing MD loads roughly equal to the average adhesion force plus the maximum applied load from the AFM experiments. This yields values of 130 nN and 150 nN for the (111) and (001) surfaces, respectively. The corresponding mean contact pressures for the infinitely stiff, curved tip (1.5 nm radius) are 65 and 55 GPa for the (111) and (001) surfaces, respectively. The contact pressure on the (001) surface is lower due to the increased contact area produced by its lower stiffness. These contact pressures are much higher than the AFM values because the tip is both smaller and infinitely stiff. According to continuum mechanics, the mean pressure scales with the tip radius R as $R^{-2/3}$, and with K as $K^{2/3}$. Despite these considerable contact pressures, no damage to the perfect diamond crystal is observed. This is reasonable, considering that the ideal shear strength of defect-free diamond is 95 GPa.[63] Tip wear is avoided completely in the simulations, and only a small amount of tip wear is observed for the 45 nm AFM tip.

Results

AFM Experiments. Friction vs load measurements were performed by alternating between crystallites corresponding to the desired combinations of surface orientation and sliding direction. Five runs were recorded at each location. Figure 4a shows data that represent a typical set of five such runs. Although there were some cases where data taken at the same location differed, the majority of the data from one location coincided, as shown in the figure. At worst, the first run at a given location exhibited slightly higher friction forces. The transient nature of

(60) Klein, C. A. *Mater. Res. Soc. Bull.* **1992**, *27*, 1407.
(61) Turley, J.; Sines, G. *J. Phys. D. Appl. Phys.* **1971**, *4*, 264.
(62) Zouboulis, E. S.; Grimsditch, M.; Ramdas, A. K.; Rodriguez, S. *Phys. Rev. B* **1998**, *57*, 2889.
(63) Roundy, D.; Cohen, M. L. *Phys. Rev. B.* **2001**, *64*, 212103.

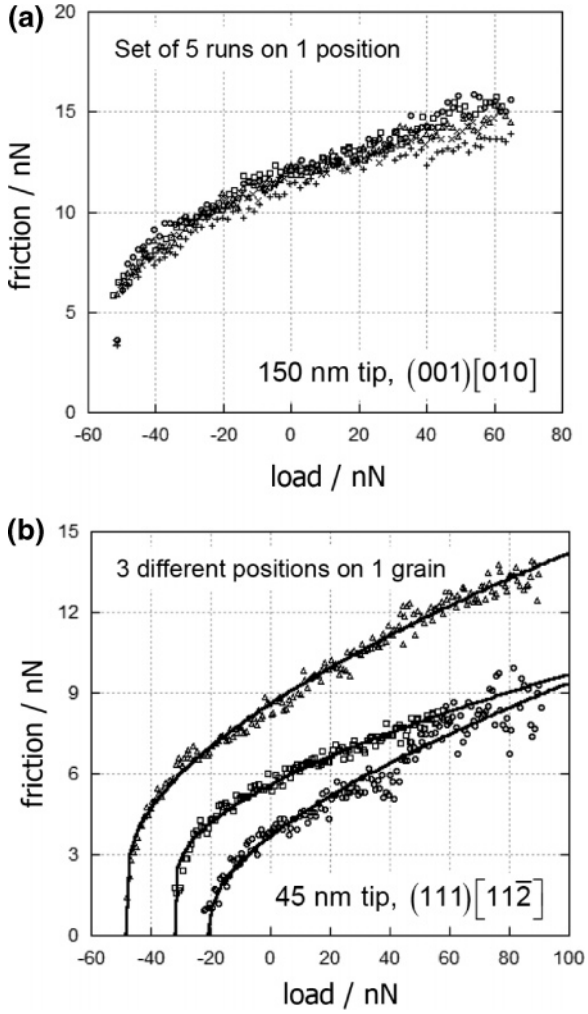

Figure 4. (a) Typical set of five AFM friction vs load runs obtained sequentially on nominally the same scan line. Tilt compensation is used, but preserving the exact location on the sample is limited by thermal drift. The different symbols correspond to each of the five runs. The data from each run exhibit impressive agreement. This particular example is for the 150 nm tip scanning in the [010] direction on a (001)-oriented grain. (b) Three averages of different friction vs load data sets (such as the set of five runs shown in panel a), depicting the type of variation in friction force observed for different locations on a given grain. This particular example is for the 45 nm tip scanning in the [11$\bar{2}$] direction on a (111)-oriented grain, beginning with the middle, lower, and then upper datasets. The curve-fits in panel b are COS transition fits (discussed in the Results section) from which work of adhesion values (γ), effective shear strengths ($\tilde{C}$), and transition parameters (α) are calculated.

these few outlying runs is suggestive of the initial presence of local, weakly bound contamination on the sample that is then removed or pushed aside by scanning, and these runs were not included in the analysis. The results of fits to individual, nontransient runs were averaged together to generate the values and uncertainties reported in Table 2.

An example of runs from three different locations is shown in Figure 4b. Each run was taken on the same (111)-oriented crystallite with the tip sliding in the [11$\bar{2}$] direction (but following alternating measurements on other crystallites). The middle, lower, and upper curves were measured in this respective order, representing the random variation observed. As Figure 4b makes evident, unlike for the sequential runs at the same location (Figure 4a), the variations between different locations on the same crystallite and for the same sliding direction are more substantial. The reason for such variations, despite using the same tip and sample, is a persistent challenge in AFM measurements that has yet to be addressed rigorously in the literature where typically only a few friction measurements are provided, and averaging, sequential measurements, error bars, and discussions of reproducibility are rarely presented. In this case, because the variations are small and infrequent for a given location, but are significant and frequent for different locations for the same grain and sliding direction, the variations must be due to surface inhomogeneities. These include adsorbed contaminants and surface chemical or structural defects such as dangling C bonds, C−O moieties, dihydride moieties, vacancies, and steps which could not be identified or avoided. These features will alter the local surface energy and the tip−sample adhesion, which is manifested in the pull-off force. Indeed, the observed variations include variations in the pull-off force, whereby lower friction forces for a given set were usually correlated with lower pull-off forces, supporting our contention that the variations are likely due to local changes in the surface structure and surface energy.[64]

As shown in Figure 2, some evolution in the 45 nm tip between the very beginning and the end of the entire set of experiments occurred. Such a limited amount of wear is impressive given the amount of sliding against diamond at appreciable loads and stresses. A larger degree of fluctuation was observed in measurements taken with the 45 nm tip than with the 150 nm tip, which may be due to the limited amount of tip wear that occurred.

Despite these variations, we found with both tips that friction forces and pull-off forces were significantly lower for (111) compared to (001) surfaces (Table 2). Pull-off forces are 43−53% lower, friction forces at zero load are 23−35% lower, and the work of adhesion (calculated using the methodology described below) is 45−60% lower on (111) compared with (001).

The lower adhesion is a manifestation of intrinsically different intermolecular interactions across the interface. In contrast, the lower friction forces on (111) surfaces could be due to a reduction either in the contact area (due to the reduced adhesive interactions, leading to less elastic deformation) or in the shear strength (due to a reduction in the intrinsic resistance to sliding that accompanies the reduced adhesion). One method to distinguish between these effects is to analyze the data using continuum contact mechanics models for the dependence of contact area on load.[65]

Continuum mechanics models have been used previously to interpret frictional behavior of nanometer-sized contacts, and impressive agreement has been found between the predicted shape of friction and stiffness vs load measurements in certain cases.[64,65] However, independent verification of the validity of continuum mechanics at this scale is lacking. Recent simulations predict that quantitative agreement should not necessarily be expected at the nanometer scale, and in some cases, the disagreement can be substantial. The MD simulations of Luan and Robbins for contact between Lennard-Jones solids and various curved tips indicate that continuum models may significantly underestimate the area of contact in nanoscale single-asperity contacts.[66] Furthermore, for the same materials, contact geometries, and loads, friction can vary dramatically due to interfacial molecular contaminants and the degree of atomic commensurability at the interface,[67−70] both of which are difficult to control in experiments. The simulations most relevant to AFM experiments used curved tips with radii in the range of 30 nm. The larger size of the AFM tips used here may enhance the validity of continuum mechanics.

(64) Carpick, R. W.; Agrait, N.; Ogletree, D. F.; Salmeron, M. *Langmuir* **1996**, *12*, 3334.
(65) Grierson, D. S.; Flater, E. E.; Carpick, R. W. *J. Adhes. Sci. Technol.* **2005**, *19*, 291.
(66) Luan, B.; Robbins, M. O. *Nature* **2005**, *435*, 03700.

However, these tips are amorphous and the substrates crystalline. Luan and Robbins predict that this case leads to the largest deviations from continuum mechanics for the contact area, assuming clean interfaces. In the AFM measurements presented here, some contaminants and water will be present despite the dry nitrogen environment, and these contaminants may counteract this disagreement.

Regardless of the exact form of the contact model, Luan and Robbins do observe that friction is related linearly to contact area for adhesive interfaces. This result depends upon the precise definition of contact area, which is ambiguous. Nevertheless, although the results for the effective shear strengths are extracted from continuum mechanics fits and may be prone to quantitative error, the comparison between different surface orientations remains meaningful. A second set of considerations, even within the framework of continuum mechanics, are the complexities such as the elastic anisotropy of the materials in contact and the effect of the applied shear stress during sliding. The anisotropy in diamond is modest. The effect of applied shear is not fully resolved, but a fracture mechanics analysis suggests it can be significant.[71,72] However, again, the effect of these corrections for the purpose of comparing different orientations of the same material using the same tip remains meaningful. Thus, we use continuum mechanics fits for the contact area and consider comparisons in the results.

There are two continuum models that provide bounds for the behavior of adhesive sphere-on-flat contacts for homogeneous, isotropic, linear elastic materials loaded purely in the normal direction. The Johnson, Kendall, and Roberts (JKR) theory is appropriate in the limit of compliant materials, large sphere radii, and strong, short-range adhesion forces.[73] In contrast, the DMT model mentioned earlier is appropriate for stiff materials, small sphere radii, and weak, long-range adhesion forces.[74] Both the JKR and DMT theories assume that the contact radius is much less than the tip radius. Many interfaces fall somewhere between the JKR and DMT limits, and this situation is accounted for by transitional models such as the Maugis-Dugdale model.[75] Simple fitting schemes, or JKR-DMT transition models, have been proposed by Carpick, Ogletree, and Salmeron (COS)[76]—and later physically justified by Schwarz[77]—for fitting AFM friction data to the Maugis-Dugdale model. In the COS representation, the transition is given by the parameter α, where $\alpha = 0$ for the DMT limit, and $\alpha = 1$ for the JKR limit. The parameter α emerges from fitting friction, F_f, vs load data to a function that describes the contact area on the basis that friction is interfacial, i.e. $F_f = \tau_0 A$. Here, the shear strength, τ_0, is assumed to be constant (i.e., independent of load). The COS transition parameter, α, is directly related to Tabor's parameter, μ_T, which can also be used to pinpoint the location of the interface on the JKR-DMT spectrum.[65,78]

The friction vs load data here were fit with the COS transition model for contact area (Figure 4b). The calibrated forces and the measured tip radii were used as inputs. The friction force at zero load and α were free parameters in the least-squares fits. The pull-off force was constrained to be the measured value. Normal forces, and therefore adhesion forces, were corrected for the relative tilt angle between the cantilever and surface of each respective grain. Occasionally, there was nonmonotonic behavior at higher loads due to the slightly imperfect tilt-compensation scheme, in which case only data at the lower loads were included in the fit. From the fits, the work of adhesion, γ, the effective shear strength, $\tilde{C}$, and α were extracted. The work of adhesion is given by $\gamma = \gamma_1 + \gamma_2 - \gamma_{12}$ where γ_1 and γ_2 are the surface free energies of each surface, and γ_{12} is the interfacial free energy.[79] From continuum mechanics, the pull-off force is directly proportional to the product of the tip radius R and the work of adhesion γ. Thus, for the same tip, differences in pull-off forces directly correlate to differences in γ. $\tilde{C}$ is related to the τ_0 via the equation, $\tilde{C} = \pi\tau_0/K^{2/3}$, where K is the combined elastic modulus of the contact, i.e. $K = 4/3((1 - \nu_{surf}^2)/E_{surf} + (1 - \nu_{tip}^2)/E_{tip})^{-1}$. E_{surf} and E_{tip} are the Young's moduli, and ν_{surf} and ν_{tip} are the Poisson's ratios for the surface and the tip, respectively. The results are shown in Table 2.

Values for $\tilde{C}$ are reported instead of τ_0 because the elastic constants of the hydrocarbon tips, and thus K, were unknown. Because the elastic constants for the (111) and (001) orientations of diamond are very close, and much larger than the tip values,[60,62] $\tilde{C}$ is a meaningful comparison of the intrinsic frictional response for different orientations when the same tip is used. Table 2 also shows a range of possible values for τ_0, which were calculated using known values for the elastic constants of diamond, the aforementioned range of reasonable values for E_{tip} (100−500 GPa), and the assumption that $\nu_{tip} = 0.3$. Note that the dependence of K on ν is very weak.

The work of adhesion measurements revealed three specific results. First, for a given tip on a given grain (i.e., surface orientation), the γ values show little variation. The total error (standard error plus experimental uncertainty) is less than 19%, and the standard error is less than 6% of the mean for a given tip-grain pair. These values are averages from 16 to 41 individual friction vs load measurements. Second, the work of adhesion observed with both tips is consistently higher for (001) than for (111) by a factor of 1.8−2.5. Third, for the same surface orientation, the small tip exhibits higher adhesion than the large tip by a factor of 2.9−4.0, depending on the surface orientation. This indicates that the small tip is chemically distinct from the large tip. Despite this significant overall difference in adhesion between the two tips, both tips exhibited higher adhesion on the (001) surfaces compared to (111).

The $\tilde{C}$ values from the transition fits are listed in Table 2. Error bars are given by the standard error of the mean plus the experimental uncertainty in the tip radius and the measured forces. Each reported $\tilde{C}$ value comes from fits to between 16 and 41 individual friction vs load measurements. For the 150 nm tip, all $\tilde{C}$ are statistically indistinguishable from each other, i.e., for the (111) [1$\bar{1}$0], (001) [$\bar{1}$10], and (001) [010] directions. For the 45 nm tip, (111)[11$\bar{2}$] and (111)[1$\bar{1}$0] are also statistically indistinguishable from each other, but $\tilde{C}$ for (001) [$\bar{1}$10] is less than (111) by 29−35%. As well, overall the $\tilde{C}$ values are significantly and consistently smaller for the 150 nm tip compared to the 45 nm tip by 12−54%, depending on the specific surface/sliding direction combination.

(67) He, G.; Müser, M. H.; Robbins, M. O. *Science* **1999**, *284*, 1650.
(68) He, G.; Robbins, M. O. *Tribol. Lett.* **2001**, *10*, 7.
(69) He, G.; Robbins, M. O. *Phys. Rev. B* **2001**, *64*, 035413.
(70) Robbins, M. O.; Muser, M. H. Computer Simulations of Friction, Lubrication, and Wear. In *Modern Tribology Handbook*; Bhushan, B., Ed.; CRC Press: Boca Raton, FL, 2001; Vol. I, p 717.
(71) Johnson, K. L. *Proc. R. Soc. London A* **1997**, *453*, 163.
(72) Kim, K. S.; McMeeking, R. M.; Johnson, K. L. *J. Mech. Phys. Solids* **1998**, *46*, 243.
(73) Johnson, K. L.; Kendall, K.; Roberts, A. D. *Proc. R. Soc. London A* **1971**, *324*, 301.
(74) Derjaguin, B. V.; Muller, V. M.; Toporov, Y. P. *J. Colloid Interface Sci.* **1975**, *53*, 314.
(75) Maugis, D.; Gauthier-Manuel, B. *J. Adhes. Sci. Technol.* **1994**, *8*, 1311.
(76) Carpick, R. W.; Ogletree, D. F.; Salmeron, M. *J. Colloid Interface Sci.* **1999**, *211*, 395.
(77) Schwarz, U. D. *J. Colloid Interface Sci.* **2003**, *261*, 99.
(78) Greenwood, J. A. *Proc. R. Soc. London A* **1997**, *453*, 1277.
(79) Israelachvili, J. N.; McGuiggan, P. M. *J. Mater. Res.* **1990**, *5*, 2223.

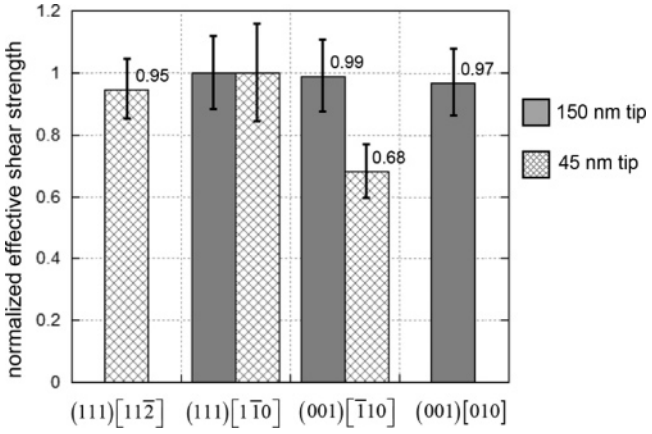

Figure 5. Bar plots of normalized effective shear strengths for the (001)- and (111)-oriented MCD grains obtained with the two tips. To compare the results for the two tips, the $\tilde{C}$ values for each tip were normalized to the value obtained for (111)[1$\bar{1}$0] with that particular tip. Surface orientations and scan directions are labeled on the horizontal axes. Error bars reflect the standard error from the experiment.

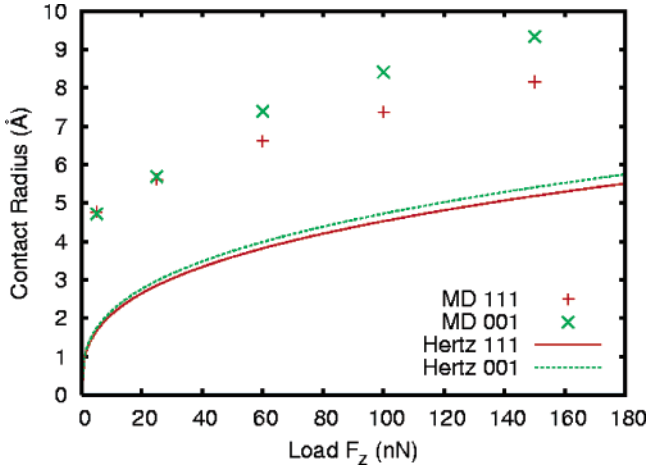

Figure 6. Contact radius as a function of load for the curved diamond tip in contact with the diamond (111)(1 × 1) -H surface and the diamond (001)(2 × 1)-H surface from MD simulations. Solid and dashed lines show the continuum predictions of the Hertz model.

The α values for the transition fits all fall between 0.5 and 1, which corresponds to values of Tabor's parameter from the fits between 1.2 and 5.3. This means that the fits place the interfaces closer to the JKR limit than to the DMT limit. However, using realistic values for the equilibrium separation and the estimated range of tip moduli, the calculated Tabor's parameter is typically less than 0.4. This disagreement between calculated and measured Tabor's parameters may be caused by a reduction in contact area due to shear forces, and has been observed previously by Carpick et al.[80] and Lantz et al.[81] and analyzed by Johnson.[71,81] It could also be due to a breakdown of continuum mechanics at these small scales. For the time being, the COS fits are used for the purpose of comparing surfaces, instead of validating a specific contact area model. In the present analysis, α is smaller on average for (111) than for (001) (∼0.6 and ∼0.9 for (111) and (001), respectively). Thus, (001) tends more toward to the JKR limit than (111), which is expected due to its stronger adhesion.

To compare all of the surface orientations and sliding directions, the relative $\tilde{C}$ for each combination is plotted in Figure 5, where each $\tilde{C}$ has been normalized to the value for the respective tip sliding on a (111) grain in the [1$\bar{1}$0] direction. The larger tip demonstrated no observable orientation effect for any of the surface orientations and sliding directions studied. However, the $\tilde{C}$ value for the 45 nm tip on the (001) surface was less than for both of the (111) measurements. The (001)(2 × 1) surface consists of dimer rows that align either perpendicular or parallel to the [$\bar{1}$10] direction. These dimers have been observed by STM[42] to exist in small domains of less than 10 nm on a single-crystal diamond surface. In this study, these structures were observed on single-crystal diamond (001) using ambient AFM but could not be resolved on MCD. Irregular stick-slip behavior is observed in all of the AFM measurements reported here. The large tip radii and 10−20 nm scan size used in this experiment would lead to multiple domains being sampled and averaged together for the [$\bar{1}$10] sliding direction.

MD Simulations. Atomic-scale friction between the two diamond tips and the diamond (111)(1 × 1)-H and (001)(2 × 1)-H surfaces was investigated using MD simulations. For the non-adhesive contact between a perfect sphere and a flat, contact mechanics predicts that the dependence of contact area with load, L, is given by $A = \pi(RL/K)^{2/3}$, where R and K are defined above.[82] To shed light on the contact between the curved diamond tip and the diamond substrates, the contact forces between the tip and the substrate atoms were calculated. The contact force on a substrate atom is the force it experiences due to all of the tip atoms. The hydrogen atoms on the surface of the diamond substrates sustain the majority of these forces, whereas the subsurface carbon atoms experience relatively small forces.

Using the method of Luan and Robbins,[66,83] the number of surface atoms with a nonzero normal force can be converted to a contact area by taking the ratio of surface atoms in contact to the total number of atoms and multiplying by the total surface area. Because the area enclosed by the surface atoms that experience a nonzero normal force is approximately circular when the curved tip is used, the contact area can be converted to a contact radius. The contact radius as a function of load for the curved diamond tip in contact with both diamond surfaces is shown in Figure 6. The continuum mechanics prediction for the contact radius as a function of load, using experimental values for the elastic constants of diamond at 300 K,[62] and the values for $E(111)$, $E(001)$, $\nu(111)$, and $\nu(001)$ for cubic materials,[61] are also shown. For loads larger than 30 nN, the contact radius for the (001) surface is always larger than the value for the (111) surface. This agrees with the continuum prediction and is a direct consequence of the fact that the Young's modulus of the (001) surface is less than the (111) surface. Although the contact radii increase with load, the MD simulations predict contact radii that are always significantly larger than the radii predicted by continuum theory.

Figure 7 shows the average friction force vs load for the curved diamond tip in sliding contact with the two diamond surfaces. When the error bars are considered, there are no statistically significant differences in friction between either surface or for any sliding direction, and friction increases monotonically with load. However, examination of the average friction (data points) reveals an interesting trend. For loads of 60 nN and above (or pressures greater than 35 GPa), the average friction force when sliding in the [$\bar{1}$10] direction on diamond (001) is always smaller than when sliding in the [110] direction. The [$\bar{1}$10] direction on diamond (001) corresponds to sliding perpendicular to the

(80) Carpick, R. W.; Agrait, N.; Ogletree, D. F.; Salmeron, M. *J. Vac. Sci. Technol. B* **1996**, *14*, 1289.
(81) Lantz, M. A.; O'Shea, S. J.; Welland, M. E.; Johnson, K. L. *Phys. Rev. B* **1997**, *55*, 10776.
(82) Hertz, H. *J. Reine Agnew. Math.* **1881**, *92*, 156.
(83) Luan, B. Q.; Robbins, M. O. *Phys. Rev. E* **2006**, *74*, 026111.

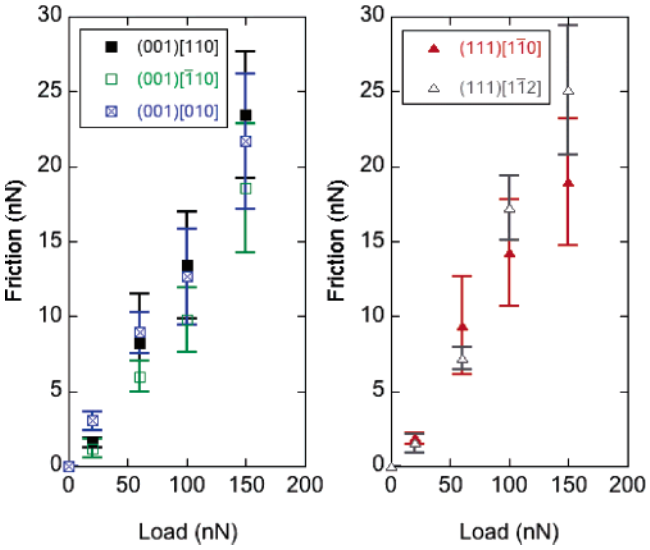

Figure 7. Average friction vs load data from the MD simulations at 300 K using the curved diamond tip. Error bars correspond to one standard deviation. Diamond surface and sliding directions are given in the legend.

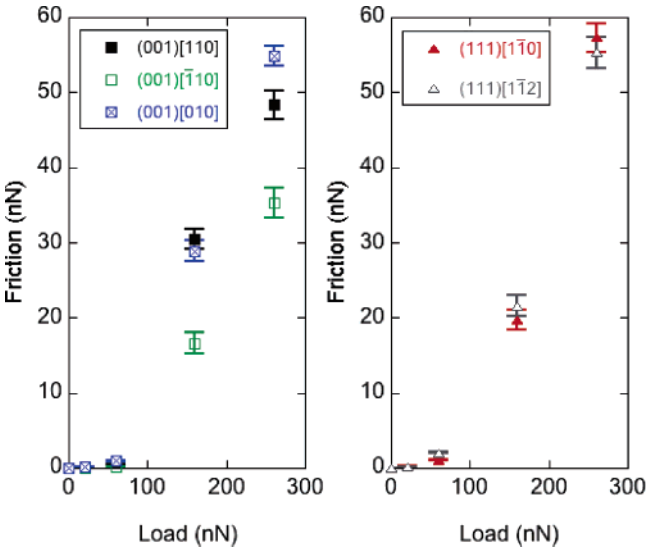

Figure 8. Average friction vs load data from the MD simulations at 300 K using the diamond nanowire tip. Error bars correspond to one standard deviation. Diamond surface and sliding directions are given in the legend.

carbon−carbon bond of the surface dimer, i.e., along the dimer rows (Figure 1).

Average friction vs load data obtained using the nanowire tip are shown in Figure 8. In this case, there is a small increase in friction at low loads followed by a more rapid and approximately linear rise beyond 60 nN (15 GPa). When the error bars are considered, the friction force in the linear region is indistinguishable for all orientations with the exception of the (001) surface when sliding in the [$\bar{1}$10] direction. This difference is most pronounced at the highest load of 260 nN.

The error bars in the friction vs load data are smaller for the nanowire tip (Figure 8) than for the curved tip (Figure 7). Because the nanowire tip is atomically flat, all of the hydrogen atoms in contact with the diamond surface experience a similar displacement during sliding and are essentially equivalent. In contrast, the hydrogen atoms on the curved tip experience a wider range of environments while sliding. This distribution of environments leads to the larger error bars associated with the curved diamond tip.

Discussion

Although the effective shear strengths measured by AFM were indistinguishable from each other for all but one case, adhesion on the (001)(2 × 1)-H surface was 78−150% greater than that on the (111)(1 × 1)-H surface. This substantial difference was observed with both tips and is important to consider for NEMS/MEMS applications where adhesion is a common mode for device failure.[84] The origin of this effect cannot be explained by considering what is known about diamond surface energies. A recent ab initio calculation of the absolute surface energies of diamond found the unreconstructed (001)-H surface to have a lower surface energy than (111)-H by nearly 1 J/m^2.[85] The (001)-(2 × 1)-H surface was not considered in that study, but it should have an even lower surface energy than the unreconstructed case. A recent ab initio calculation found that there is an increased amount of polarization of the C−CH and C−H bonds on the (001)(2 × 1)-H surface compared to that of the (111)(1 × 1)-H surface,[86] and this could affect adhesion forces measured by AFM by enhancing electrostatic interactions. Further verification with measurements in UHV would eliminate the possibility that water or contamination is contributing to the result.

The $\tilde{C}$ values were similar for both (111) and (001) surfaces when using the 150 nm tip. Furthermore, $\tilde{C}$ for the 45 nm tip was actually somewhat smaller on the (001) surface, even though the adhesion contrast between the two surface orientations was greatest for this tip. In other words, the surface crystallographic orientation determines the work of adhesion and friction forces, but these increases can be attributed to an increase in contact area induced by higher adhesion, as opposed to an increase in $\tilde{C}$ or the shear strength. The two surfaces, therefore, show no difference in the intrinsic resistance to shear (friction force per unit area, i.e., per interfacial atom).

The values of $\tilde{C}$ for the two AFM tips were significantly different (by a factor of ∼2 excluding the anomalous case of (001)[1$\bar{1}$0] with the 45 nm tip) with the 150 nm tip exhibiting lower values than the 45 nm tip (Table 2). This contrast may have several origins. First, the tip modulus and surface chemistry may vary for each EBID growth, leading to variability in the shear strength. Indeed, the work of adhesion values were very different for the two tips (see Table 2). The origin of this difference in adhesion is unknown, but could be due to different degrees of oxidation of the surface of the EBID tip coating resulting from having different densities of unsaturated surface bonds at the end of the EBID growth. Regardless, the more adhesive nature of the smaller tip may lead to a higher shear strength, which has been observed in numerous cases.[27,64,87] The tip modulus may be affected by that of the underlying tungsten carbide, and this effect may be more significant for the smaller tip, which has a thinner hydrocarbon coating. Moreover, Kim and Hurtado[88] have predicted that the shear strength should increase as the tip radius decreases, based on a dislocation-assisted slip model.[89,90] The measured difference in adhesion between the two tips, and the uncertainty in applying a dislocation-based model to a system

(84) Maboudian, R.; Ashurst, W. R.; Carraro, C. *Tribol. Lett.* **2002**, *12*, 95.
(85) Stekolnikov, A. A.; Furthmuller, J.; Bechstedt, F. *Phys. Rev. B* **2002**, *65*, 115318.
(86) Urban, J. unpublished results.
(87) Enachescu, M.; Carpick, R. W.; Ogletree, D. F.; Salmeron, M. *J. Appl. Phys.* **2004**, *95*, 7694.
(88) Kim, K. S.; Hurtado, J. A. *Fracture Strength Solids, Pts. 1 & 2, Key Eng. Mater.* **2000**, *1*, 183−1.
(89) Hurtado, J. A.; Kim, K.-S. *Proc. R. Soc. London A.* **1999**, *455*, 3384.
(90) Hurtado, J. A.; Kim, K. S. *Proc. R. Soc. A* **1999**, *455*, 3363.

with one amorphous surface (the tip), prevents us from directly assessing if this mechanism is at play. Although the dependence of friction on tip size has not yet been modeled atomistically for this system, Muser et al. have determined that friction for microscopic contacts diminishes with increasing contact size, due to cancellation of random fluctuations.[91] This effect would lead to smaller shear strengths for larger tips, in agreement with our results.

Schwarz et al. have previously reported average values for $\tilde{C}$ of (001)-oriented MCD for five EBID-coated tips.[26] The mean $\tilde{C}$ values in air and argon were 0.263 ± 0.060 and 0.158 ± 0.061 $N^{1/3}nm^{-2/3}$, respectively. These values are an order of magnitude greater than the values reported here. Some difference could be due to force calibration procedures, which have been significantly improved for AFM over the years. In addition, the MCD films in their work were not deliberately hydrogen terminated, and unsaturated bonds, oxidized bonds, and other defects or contaminants on the surface could increase the effective shear strength. There may also have been a significant difference in tip chemistry or Young's modulus compared with the present experiments, because the EBID processes are not identical. Finally, different, and mostly smaller, tip radii were used by Schwarz et al., although not all of the values are reported. It is possible that the larger shear strengths are a result of a smaller contact, as predicted by Kim and Hurtado's, and Müser's, models.

Because the Young's moduli and Poisson's ratios of the tips are unknown, τ_0 cannot be determined precisely. However, using $\nu_{tip} = 0.3$ and the range of reasonable values for E_{tip} stated previously yields the range of shear strengths shown in Table 2. They are within reasonable limits and within range of the 238 MPa shear strength measured for a 110 nm radius tungsten carbide tip on H-terminated diamond in UHV.[24,25] It would be extremely unusual for shear strengths to exceed the ideal shear strength of the tip or sample, because in such a case the materials should yield before the interface slips. These can be estimated to be $\sim G/30$, where G is the shear modulus of the tip or sample.[88] Estimates for $G/30$ are also given in Table 2, and they fall well above the estimated shear strengths.

Although there were differences in both adhesion and radius between the two AFM tips used in this work, no dependence of $\tilde{C}$ on sliding direction was observed using either tip, except for the case of the small tip on the (001)[1$\bar{1}$0] orientation. That this is otherwise consistent for two tips of different size (and therefore different contact pressures at the same loads) and different tip chemistries suggests that the sliding direction truly has no impact on the shear strength of hydrogen-terminated diamond surfaces, with the one exception mentioned above.

This exception may be explained by the MD simulations. According to the AFM results, the larger tip shows no difference between effective shear strengths for (111) and (001) surfaces, whereas the smaller tip exhibits intrinsically lower resistance to sliding (by a factor of $\sim$0.7) for (001)[1$\bar{1}$0] compared to all others, despite higher adhesion on (001). At most of the higher loads, the MD simulations with both tips also predict lower overall average friction (data points) when sliding perpendicular to the C−C bond, and friction comparable to all other orientations when sliding parallel to the C−C bond (Figure 7). When the nanowire tip is used, the difference in friction is outside the error bars. Averaging dimer domains together, which we expect to occur in the AFM experiments, would still lead to a lower overall friction for (001)[1$\bar{1}$0] at high contact pressures. This may explain the surface orientation dependence observed for the 45 nm tip, for which there were greater overall contact pressures due to the smaller radius and higher adhesion.

Although we caution that the tip sizes, contact pressures, sliding speeds, and precise atomic structures of the tips used in the MD simulations and the AFM experiments are different, the results are, nonetheless, essentially in agreement. First, for comparable ranges of loads, the friction forces are comparable in magnitude for both MD and AFM. Net loads (with respect to tip−sample separation) of 0−150 nN correspond to friction forces in the range of 5−20 nN. Second, the simulations and experiments agree that there is essentially no directional dependence to the friction force on the diamond (111) surface. The simulations predict that the friction force when sliding parallel to or at 45° to the carbon−carbon dimer bonds on diamond (001)(2×1) is comparable to that obtained on the diamond (111) surface. The AFM experiments are consistent with this MD result.

In addition, the MD simulations predict that sliding perpendicular to the C−C dimer bonds on diamond (001) (along the [$\bar{1}$10] direction) yields lower average friction at high loads than when sliding parallel to the bonds (the [110] direction) under certain conditions. Changing the tip geometry from curved to flat exacerbates this difference. These simulations demonstrate that the tip shape, and perhaps size, can mask or enhance this friction difference as was also demonstrated in the AFM experiments. The MD simulations also lend additional insight into the mechanism behind this difference in friction. Simulations have shown that one mode of frictional energy dissipation in diamond is the vibrational excitation of bonds due to the interactions of the hydrogen atoms on opposing surfaces.[33,37] The amount of the vibrational excitation imparted to the hydrogen atoms depends largely upon the applied load and the space constraints within the contact. The more steric freedom the hydrogen atoms have to move out of the way of the sliding counterface, the lower the vibrational excitation and thus the friction. The larger spacing between the surface hydrogen atoms perpendicular to the dimer bond allows the surface hydrogen atoms more freedom, depending upon the contact geometry of the tip, and thus friction can be lower when sliding in this direction. A second contribution could be due to the overall increased corrugation of the surface potential along the dimer bond, due to the dimer rows and the troughs between them (Figure 1a), which increases the potential barrier that must be overcome to initiate sliding, and increases the probability of stick-slip energy dissipation. Such frictional anisotropy has been previously observed for anisotropic polymer monolayers whereby the more corrugated direction yielded higher nanoscale friction.[92] Friction vs load measurements on individual dimer domains are necessary to fully understand the effect of sliding direction on the (001) surface and to test the MD prediction that sliding parallel to the carbon−carbon bonds can result in higher friction for certain tip geometries. We are currently attempting to resolve individual dimer domains using UHV experiments, smaller tips, and single-crystal surfaces.

While the AFM measurements and MD simulations are essentially in agreement regarding the dependence of friction on crystallographic surface orientation and sliding direction, the shapes of the friction vs load curves differ. In the AFM experiments, adhesion results in a nonzero friction force at zero applied load. Because all of the surfaces are hydrogen-terminated in the simulations, there is no chemical adhesion between the surfaces. In addition, the potential used in the MD simulations does not allow for van der Waals forces between the surfaces.

(91) Muser, M. H.; Wenning, L.; Robbins, M. O. *Phys. Rev. Lett.* **2001**, *86*, 1295.

(92) Moseler, M.; Gumbsch, P.; Casiraghi, C.; Ferrari, A. C.; Robertson, J. *Science* **2005**, *309*, 1545.

In the low-load regime, the AFM data possess a modest, reproducible curvature that is not apparent in the MD data. As shown by the fits in Figure 4b, this curvature is consistent with the nonlinear increase in contact area with load that continuum mechanics predicts. The MD results for the spherical tip indeed give a nonlinear contact area vs load relation (Figure 6), although the dependence differs from the continuum mechanics predictions. However, friction for the spherical tip is nearly linear with load (Figure 7) in all the MD simulations. In contrast, the friction vs load data produced by the nanowire tip are nonlinear with loads below ~60 nN producing very little friction. The Tomlinson model[93] predicts that the kinetic friction is essentially zero until the stiffness of the interfacial potential exceeds that of the remainder of system. Because the simulations are much stiffer than the experiments, this effect should not occur in the AFM experiments. This is one possible explanation for the nonlinearity of the friction vs load data.

Approximately linear friction vs load behavior has been observed previously with MD[31] and ab initio simulations that examined friction between self-mated, infinitely flat hydrogen-terminated diamond surfaces.[32] Although the curvature of friction vs load data in the negative-load regime is apparent in many AFM experiments of solid−solid contacts, cases have been reported where these data are linear.[94,95] Recently, linear friction vs load data were measured in UHV for a silicon tip in contact with a (111) silicon wafer.[95] In that work, the adhesion between the tip and the sample was small, though no effort was made to quantify the shape or size of the tip.

Recently, MD simulations have been used to examine the conditions that lead to linear and nonlinear friction vs load behavior in nanoscale contacts.[83,96] In both of these studies, pure Lennard-Jones interaction potentials were used. Wenning and Müser[96] used a tip with a 3 nm radius and Luan and Robbins used tips with radii that were an order of magnitude larger. In both cases, commensurate tip−sample contact in the absence of adhesion yielded the situation where $F_f \propto L$ and incommensurate contacts produced the common $F_f \propto L^{2/3}$ behavior. In addition, analytic[91] and numerical[97] models have demonstrated that the linear dependence of friction with load is a general feature of commensurate surfaces. Furthermore, Wenning and Müser concluded that the relatively large contact radii present in AFM tips may lead to a degree of self-averaging. This would result in the nonlinear friction vs load behavior that is similar to that produced by the MD simulation of an incommensurate tip−surface contact. Although it is encouraging that linear friction versus load behavior has been observed in other simulations, linear behavior is observed for both the commensurate and incommensurate contacts presented here. It is possible that either the short-range nature or the directional bonding of the REBO potential is the origin of the differences between this work and the work described above. It is clear that the origins of linear vs nonlinear friction load behavior, the connection with contact area, and the breakdown of continuum mechanics, requires further study both experimentally and through simulations and theory.

Summary

In summary, wearless friction between nanoscale tips and diamond (111)(1 × 1)-H and (001)(2 × 1)-H surfaces was examined using both AFM and MD. Particular attention was paid to making the correspondence between the AFM experiment and the simulations as close as state-of-the-art techniques allow. We found that the adhesion and friction forces were higher for (001) surfaces compared to (111) in the AFM experiments. The difference in friction forces can be explained entirely by the difference in contact area that arises from the contrast in adhesion. Because the elastic constants of the AFM tip were unknown, the intrinsic frictional response, represented by an effective shear strength, was used to compare orientations and make qualitative comparisons with the simulations. The experiments and simulations agree that the intrinsic frictional response on both diamond surfaces is similar at low pressures. In contrast to macroscopic behavior involving wear, there was no direction dependence to the wearless friction studied here, with one exception. The MD simulations predicted that friction on the diamond (001)(2 × 1)-H surface should be less when sliding perpendicular to the carbon−carbon bond vs parallel to it. The size of the dimer domains on the diamond (001)(2 × 1)-H surface and the large size of the AFM tips limited the experimental verification of this prediction. However, the smaller AFM tip gave evidence for a lower friction response on average for the (001) surface, suggesting that the dimer orientation effect predicted by MD may indeed be manifested in the experiments. Experiments are currently underway to verify this rigorously using single-crystal surfaces and smaller tip radii in UHV.

Acknowledgment. G.G. acknowledges support from the Air Force Office of Scientific Research (AFOSR) as part of the Extreme Friction MURI (FA9550-04-1-0381 and F1ATA06355G004). J.A.H. acknowledges partial support from AFOSR (F1ATA06306G001) and from the Office of Naval Research (N0001407-WX-20904). R.W.C. and R.J.C. acknowledge support from the NSF CAREER Award No. CMS 0134571, and the AFOSR Grant No. FA9550-05-1-0204. R.W.C. and R.J.C. are grateful to Suresh Vagarali of GESuperabrasives, General Electric Company, for providing the micro-diamond powders used in this work. In addition, R.J.C. is grateful to Anirudha Sumant for his active contribution in the preparation and growth of the MCD films used in this work. R.J.C. and R.W.C. acknowledge the assistance of Graham Wright and Dennis Whyte (University of Wisconsin−Madison) for ERD analysis of the diamond surfaces, and Katherine Cimatu and Steven Baldelli (University of Houston) for SFG analysis of the diamond surfaces. We also thank U. D. Schwarz, R. S. Ruoff, M. O. Robbins, and H. I. Kim for helpful discussions.

LA062254P

(93) Tomlinson, G. A. *Phil. Mag.* **1929**, *7*, 905.
(94) Mate, C. M. *Wear* **1993**, *168*, 17.
(95) Schirmeisen, A.; Jansen, L.; Holscher, H.; Fuchs, H. *Appl. Phys. Lett.* **2006**, *88*, 123108.
(96) Wenning, L.; Muser, M. H. *Europhys. Lett.* **2001**, *54*, 693.
(97) Ringlein, J.; Robbins, M. O. *Am. J. Phys.* **2004**, *72*, 884.